Supporting Information:

Evidence for H_2-induced ductility in a Pt/Al_2O_3 catalyst

Eleonora Vottero[a,b]*, Michele Carosso[a], Alberto Ricchebuono[a], Monica Jiménez-Ruiz[b], Riccardo Pellegrini[c], Céline Chizallet[d], Pascal Raybaud[d,] Elena Groppo[a] and Andrea Piovano[b]

Affiliations

[a] Department of Chemistry, INSTM and NIS Centre, University of Torino, via Quarello 15, I-10135 Torino, Italy

[b] Institut Laue-Langevin (ILL), 71 avenue des Martyrs, 38042 Grenoble, France

[c] Chimet SpA - Catalyst Division, Via di Pescaiola 74, I-52041, Viciomaggio Arezzo, Italy

[d] IFP Energies nouvelles, Rond-point de l'échangeur de Solaize, BP3, 69360 Solaize, France

*eleonora.vottero@unito.it

S1: Further details on the residual Pt-H after reduction

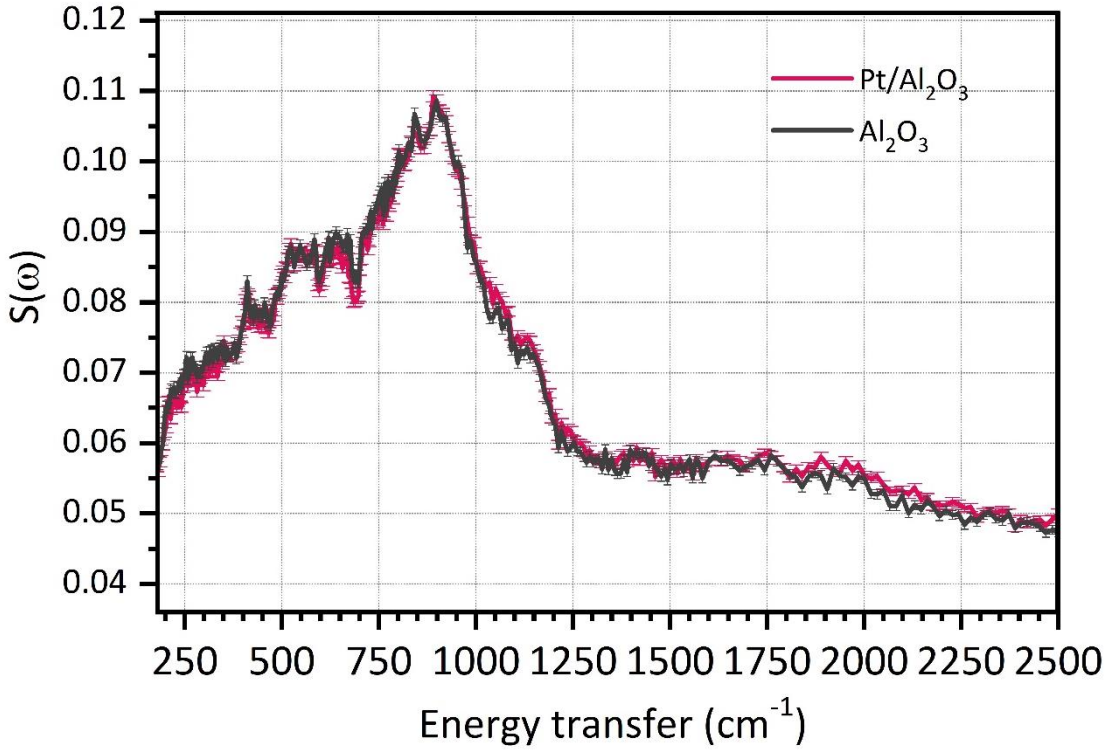

Figure S 1: Comparison between the INS spectrum of the Pt/Al_2O_3 activated by outgassing and reduction at 393 K, and of the bare Al_2O_3 support after treatment at 393 K in vacuum. Few residual Pt-H could remain on the catalyst following the activation treatment, but the very good match between the two spectra indicates that they are either absent, or present at very low concentrations not detectable at the current spectral resolution.

S2: Details over the Bose-Einstein correction of the spectra

The temperature at which the INS spectra are measured affects the resulting profiles, in particular in the low energy transfer range. So that the two experiments described in this work were performed at different temperatures, we have to take into account this factor to be able to compare the resulting spectra. For doing so, we corrected the spectral profile for the Bose-Einstein factor which considers the different population of the vibrational energy levels as a function of the temperature.
The formula employed for the spectra correction is the following:

$$S(\omega)_{corrected} = \frac{S(\omega)_{uncorrected}}{n_{Bose\text{-}Einsten}(\omega) + 1} \qquad (i)$$

where $n_{Bose\text{-}Einsten}(\omega)$ corresponds to:

$$n_{Bose\text{-}Einsten}(\omega) = \frac{1}{\exp(\omega\ 11.6045/T) - 1} \qquad (ii)$$

where T is the temperature in K, ω is the energy transfer in meV, and 11.6045 accounts for the unit conversion from meV to J divided for the Boltzmann constant.

This correction factor was applied to the spectra collected during experiment (2), in which the sample was measured at a temperature of 453 K. The spectra collected during experiment (1) instead, for which the measurement temperature corresponded to 25 K, did not require a correction as the corrective factor was basically equal to 1.
The original spectra for experiment (2) and the ones obtained after the Bose-Einstein correction are shown in Figure S 2.

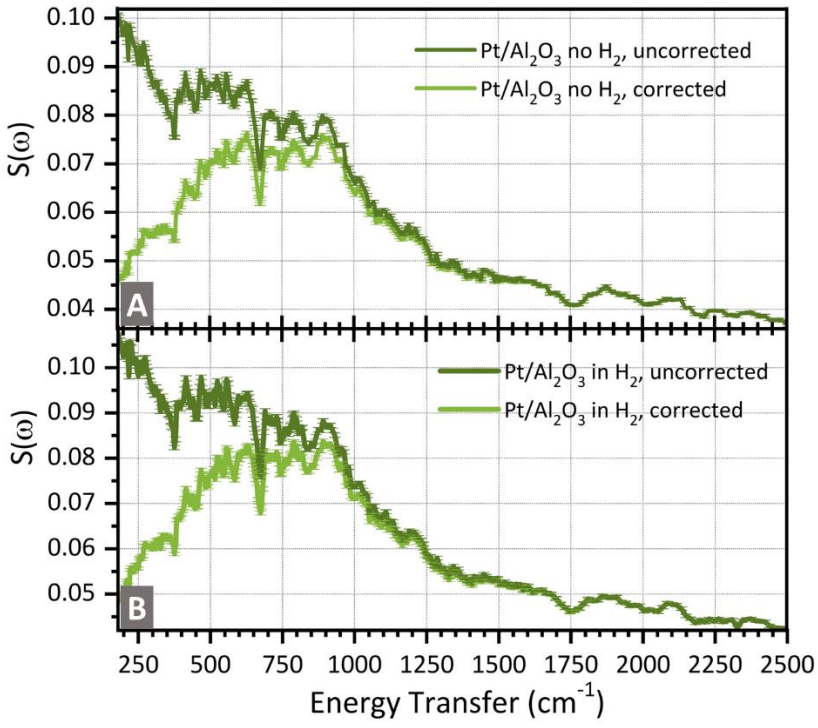

Figure S 2: comparison between the original (dark green) and corrected (light green) spectra for the Pt/Al_2O_3 sample measured as such (part A) and in the presence of a small amount of H_2 (part B) at 450 K.

S3: Computational details of the models

In this section, further details over the models employed for the INS spectra simulations will be provided.

The structure of the dehydroxylated γ-Al_2O_3 (100) surface and partially hydroxylated γ-Al_2O_3 (110) one (8.9 -OH nm^{-2}) employed as support in the current work are the ones described and optimised in refs 1-3. The chosen -OH coverage for the two surfaces corresponds to the most stable one under typical reaction conditions (above 600 K), as obtained from thermodynamic calculations.[2] In both cases the support was simulated as a 4-layers thick slab.

To avoid lateral interaction between the supported nanoparticles, 2x2 (for (110)) or 3x2 (for (100)) supercells of the support were employed. The final models were obtained by placing Pt_xH_y clusters on top of this support supercell. The classification of all the models considered, the cell parameters and the process employed for optimizing their structures are summarised in Table S 1.

Table S 1: summary of the models considered in the present work.

	Models included	**Cell parameters**	**Optimization method**
$Pt_{13}H_y$/γ-Al_2O_3 (100)	$Pt_{13}H_2$, $Pt_{13}H_4$, $Pt_{13}H_6$, $Pt_{13}H_8$, $Pt_{13}H_{10}$, $Pt_{13}H_{12}$, $Pt_{13}H_{14}$, $Pt_{13}H_{16}$, $Pt_{13}H_{20}$, $Pt_{13}H_{32}$, $Pt_{13}H_{34}$	a = 16.714 Å b = 16.787 Å c = 21.800 Å	The most stable geometries for the supported Pt_{13} clusters at various H coverages were screened through velocity scale molecular dynamics calculations as described in[4, 5] and then fully optimised at 0 K to an energy minimum (convergence criterion: $2*10^{-2}$ eV/Å). These models correspond to the ones already described in ref[5].
$Pt_{13}H_y$/γ-Al_2O_3 (110)	$Pt_{13}H_0$, $Pt_{13}H_2$, $Pt_{13}H_8$, $Pt_{13}H_{16}$, $Pt_{13}H_{20}$, $Pt_{13}H_{36}$	a = 16.144 Å b = 16.787 Å c = 25.000 Å	The most stable geometries for the supported Pt_{13} clusters at various H coverages were screened through velocity scale molecular dynamics calculations as described in[4, 5] and then fully optimised at 0 K to an energy minimum (convergence criterion: $2*10^{-2}$ eV/Å). These models correspond to the ones already described in ref[4].
Pt_xH_y/γ-Al_2O_3 (100) (x = 34, 38, 55)	$Pt_{34}H_{54}$, $Pt_{38}H_{64}$, $Pt_{38}H_{72}$, $Pt_{55}H_{44}$, $Pt_{55}H_{81}$ (2 isomers) $Pt_{55}H_{91}$ (2 isomers) $Pt_{55}H_{116}$	a = 16.714 Å b = 16.787 Å c = 30.000 Å	These clusters were obtained by cutting the desired regular shape from the bulk Pt lattice, by locating the obtained cluster on the support and adding the intended amount of H atoms. The structures were then fully optimised at 0 K to an energy minimum (convergence criterion: $2*10^{-2}$ eV/Å).

We focused on Pt cluster of comparable size with the one determined by TEM in our sample (1.4 ± 0.4 nm).[6] The models diameters were evaluated by measuring the Pt-Pt core-to-core distances between atoms at the extremes of the cluster, averaging the values obtained along different axis in the model. To compare these values with TEM, we then added the value of the van der Waals radius

for Pt (175 pm) to the two extreme atoms. Some representative models' size evaluated following this procedure are reported in Table S 2.

Table S 2:simulated Pt clusters sizes as evaluated by measuring the average core-to-core distance and by also considering the van der Waals Pt radii for a representative set of Pt_xH_y models.

	Core-to-core size (nm)	**Size considering VdW radii (nm)**
$Pt_{13}H_{16}/\gamma\text{-}Al_2O_3$ (100)	0.58	0.93
$Pt_{13}H_{32}/\gamma\text{-}Al_2O_3$ (100)	0.56	0.91
$Pt_{34}H_{54}/\gamma\text{-}Al_2O_3$ (100)	0.86	1.21
$Pt_{38}H_{72}/\gamma\text{-}Al_2O_3$ (100)	0.90	1.25
$Pt_{55}H_{44}/\gamma\text{-}Al_2O_3$ (100)	1.03	1.38
$Pt_{55}H_{81}/\gamma\text{-}Al_2O_3$ (100)	1.14	1.49
$Pt_{55}H_{91}/\gamma\text{-}Al_2O_3$ (100)	1.11	1.46

S4: Further details on the linear combination fit procedure

The experimental difference spectrum containing the fingerprint of the Pt-H species formed under $P(H_2)$ of 160 mbar and at room temperature, measured during experiment (1) and shown in Figure 3B in the main text, was fitted with a linear combination of simulated spectra. The fit was calculated by using an iterative nonlinear fitting algorithm, in which each simulated function was multiplied by a weight coefficient whose value was optimised to minimize the sum of squared residuals between the experimental spectrum and the fit solution. The final values of these multiplicative weight coefficient were then used for calculating the percentage of each simulated spectrum in the fitted solution, which corresponds to the predicted percentage of hydrogenated nanoparticles corresponding to that models in the experimental spectrum.

Considering that the frequency calculation by means of finite displacements implicitly employs the harmonic approximation, which is known to lead to a slight overestimation of the vibrational frequencies in comparison with the experimental ones,[7] a small scaling factor multiplying the calculated frequencies was also introduced and optimized in the fit. The same scaling factor was applied to all the simulated functions included in the fit, and it was constrained within the $0.99 < s < 1.01$ range.

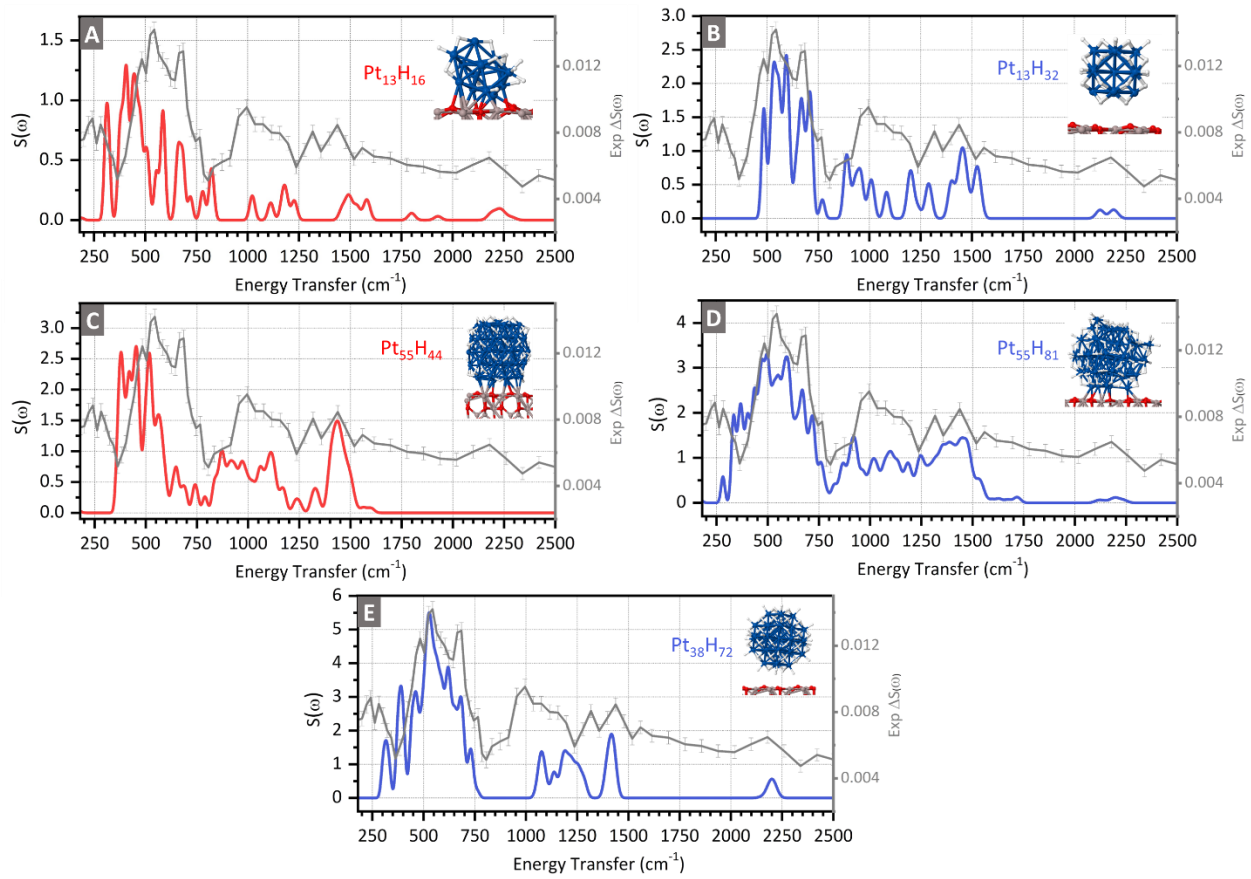

Figure S 3: Selection of representative comparisons between the simulated and experimental spectrum containing the fingerprint of the Pt-H species formed under high H-coverage conditions employed for selecting the models to be included in the linear combination fit analysis. The spectra plotted in red were eventually excluded from the final fit, while the blue ones were selected.

Only few simulated functions were included in the fit, to ensure the convergence of the calculation and avoid artifacts arising from the introduction of functions too similar to each other.

A first screening of the functions was done by qualitatively comparing the simulated and experimental spectral profiles and excluding the ones not showing a satisfying agreement level (in particular regarding the position of the main bands in the spectra and their correspondence with the experimental spectrum to be fitted), as shown in Figure S 3. Other functions were excluded when performing some preliminary linear combination fit tests, as their weight to the final fit solution was equal or lower to 1%.

In the case of the $Pt_{55}H_{81}$ and $Pt_{55}H_{91}$ models, two isomers for each stoichiometry were considered (Figure S 6A, A', B, B'), whose spectra show quite similar spectral features (in particular in terms of the bands position). In this case, the preliminary test fits were not converging when considering the simulated spectra of both the isomers at the same time, probably because their spectral features are too similar. On the other hand, the test runs made by including only one isomer at a time indicated that both the isomers gave very similar percentages in the final fit results, not allowing us to choose a function over the other. Thus, it was decided to calculate the average spectrum between the two forms and to include this average function into the fit for both the couples of isomers.

S5: Detail over the contribution of top-bridge and interfacial top Pt-H species

Some representative examples of the geometric and spectral features of top-bridge and interfacial top Pt-H species are shown in Figure S 4.

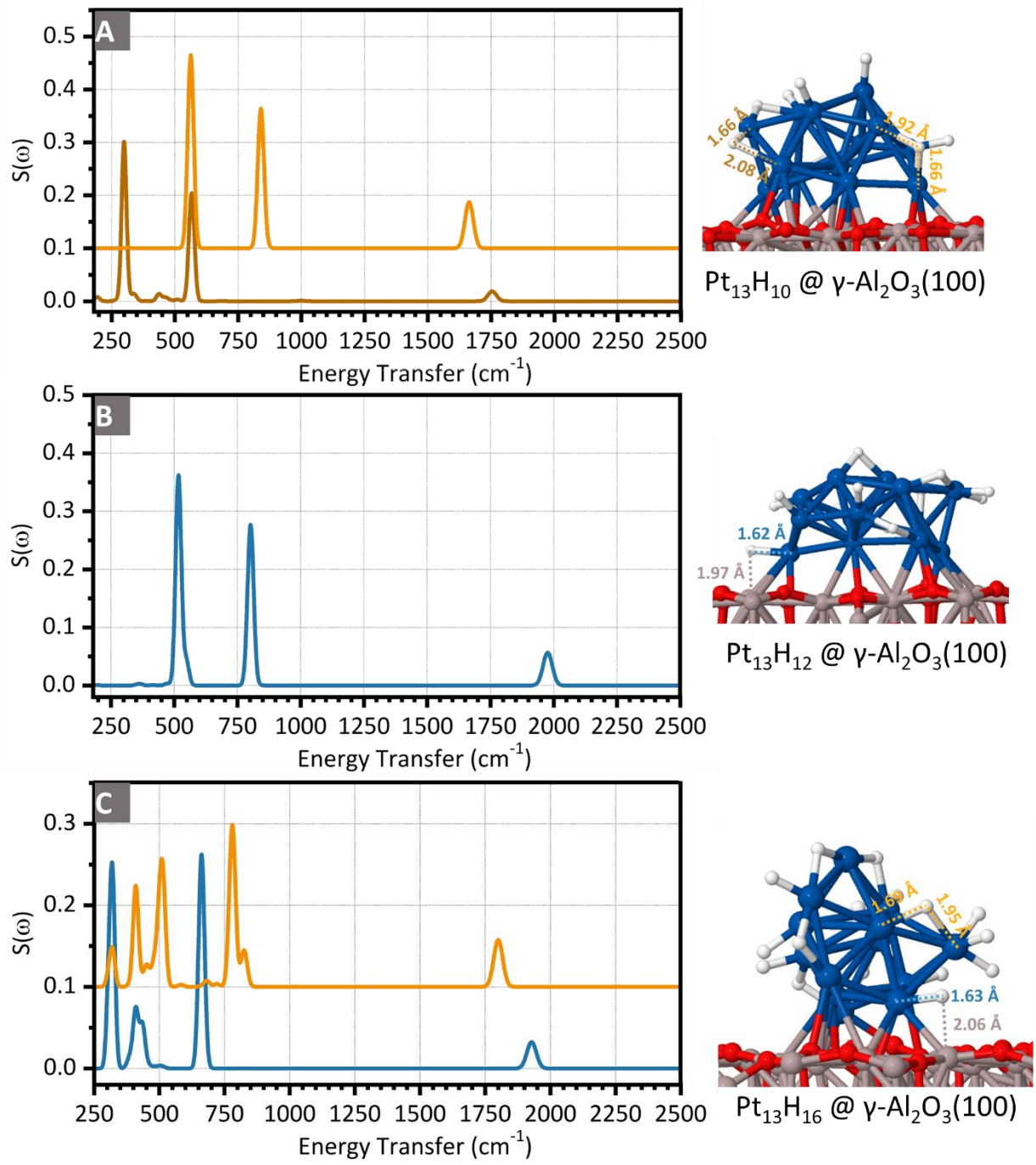

Figure S 4: Spectral contributions of top-bridge Pt-H species to the INS spectra (orange plots) and of interfacial top Pt-H species (blue plots) for models $Pt_{13}H_{10}$ (A), $Pt_{13}H_{12}$ (B) and $Pt_{13}H_{16}$ (C). The geometries of the three models and the relevant bond lengths are also indicated.

S6: Simulated INS spectra of all the models

The simulated INS spectra of the models not included in Figure 5 in the main text are reported in Figure S 5, Figure S 6 and Figure S 8 in the current section.

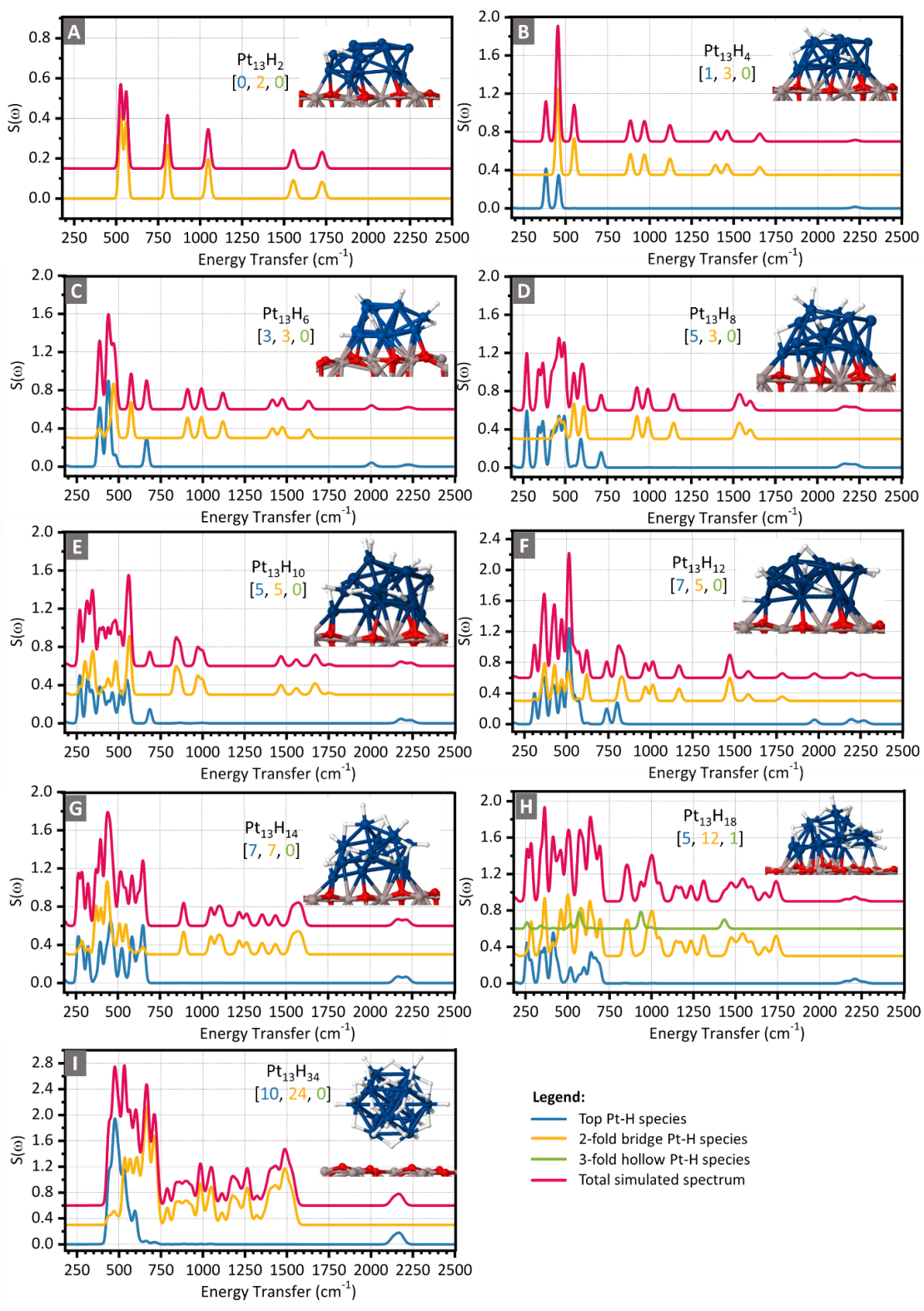

Figure S 5: simulated spectra of the models $Pt_{13}H_2$ (A), $Pt_{13}H_4$ (B), $Pt_{13}H_6$ (C), $Pt_{13}H_8$ (D), $Pt_{13}H_{10}$ (E), $Pt_{13}H_{12}$ (F), $Pt_{13}H_{14}$ (G), $Pt_{13}H_{16}$ (H), $Pt_{13}H_{34}$ (I) supported at the dehydroxylated γ-Al_2O_3 (100) surface. The number of Pt-H of each type is indicated in the form [top, bridge, hollow].

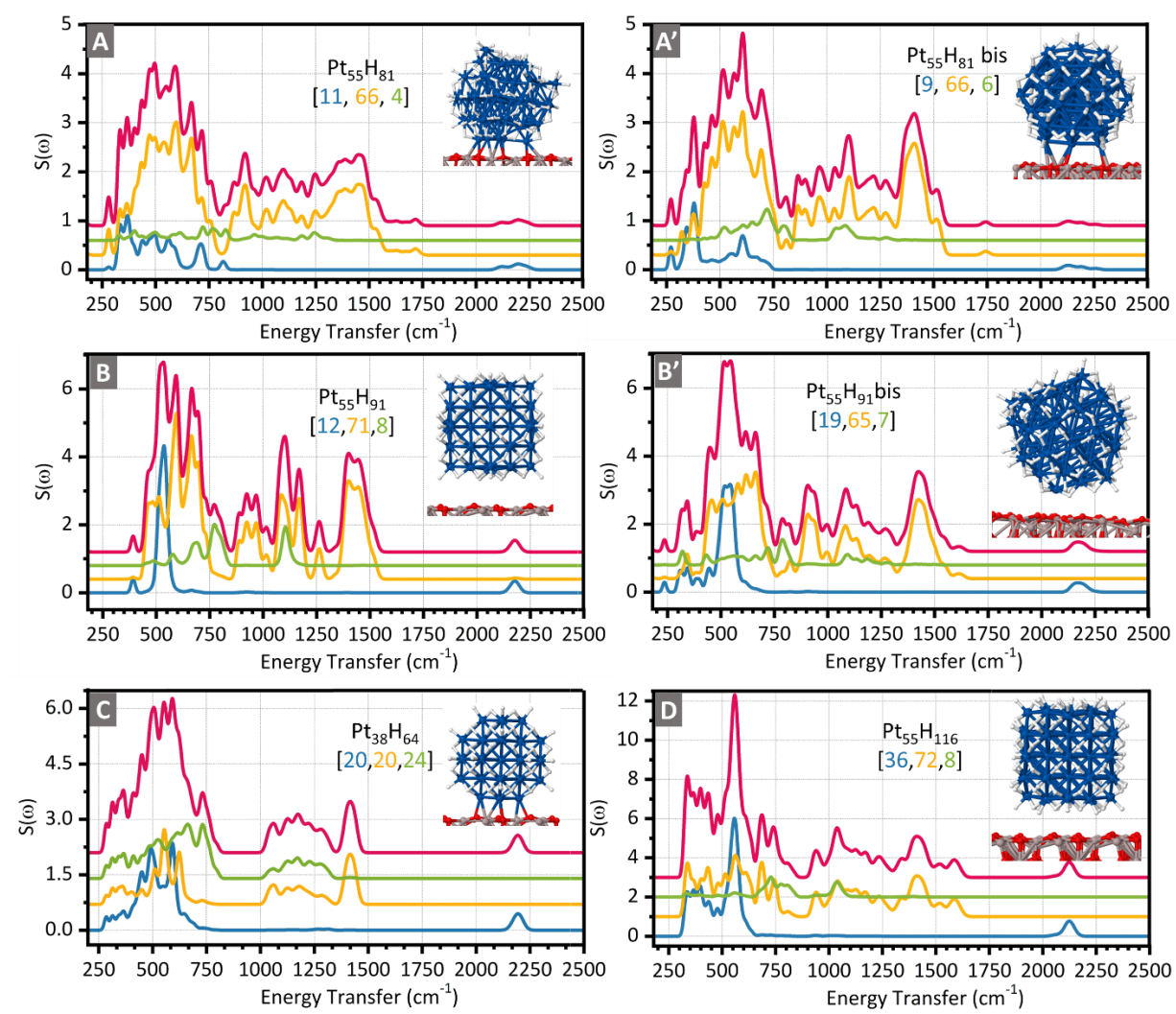

Figure S 6: simulated INS spectra of the two $Pt_{55}H_{81}$ isomers (A and A'), of the two isomers of $Pt_{55}H_{91}$ (B and B'), of $Pt_{38}H_{64}$ (C) and of $Pt_{55}H_{116}$ (D). All the models are supported on the dehydroxylated γ-Al_2O_3 (100) surface. The number of PtH of each type is indicated in the form [top, bridge, hollow].

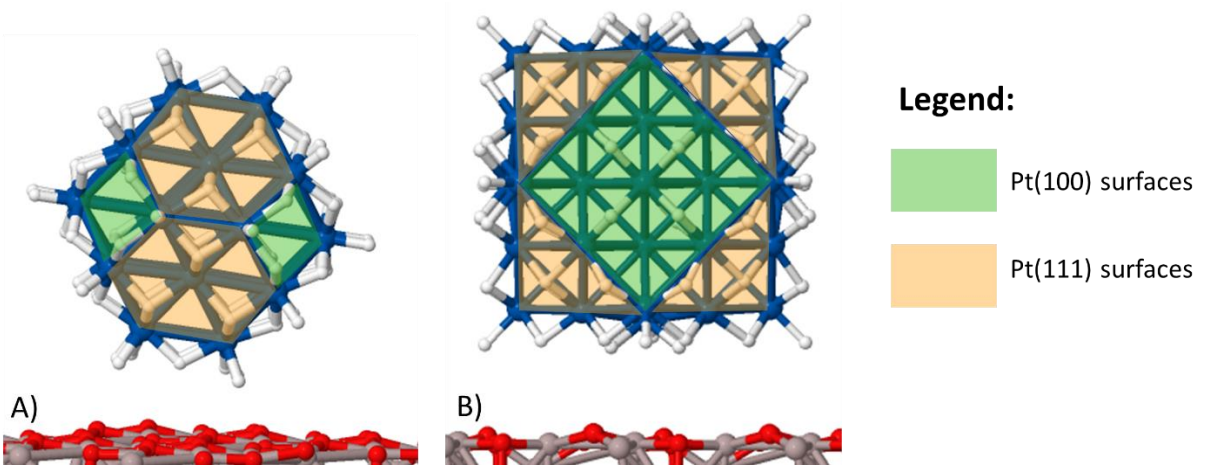

Figure S 7: detail over the exposed surfaces in the truncated octahedra $Pt_{38}H_y$ models (A) and cuboctahedric $Pt_{55}H_y$ ones (B).

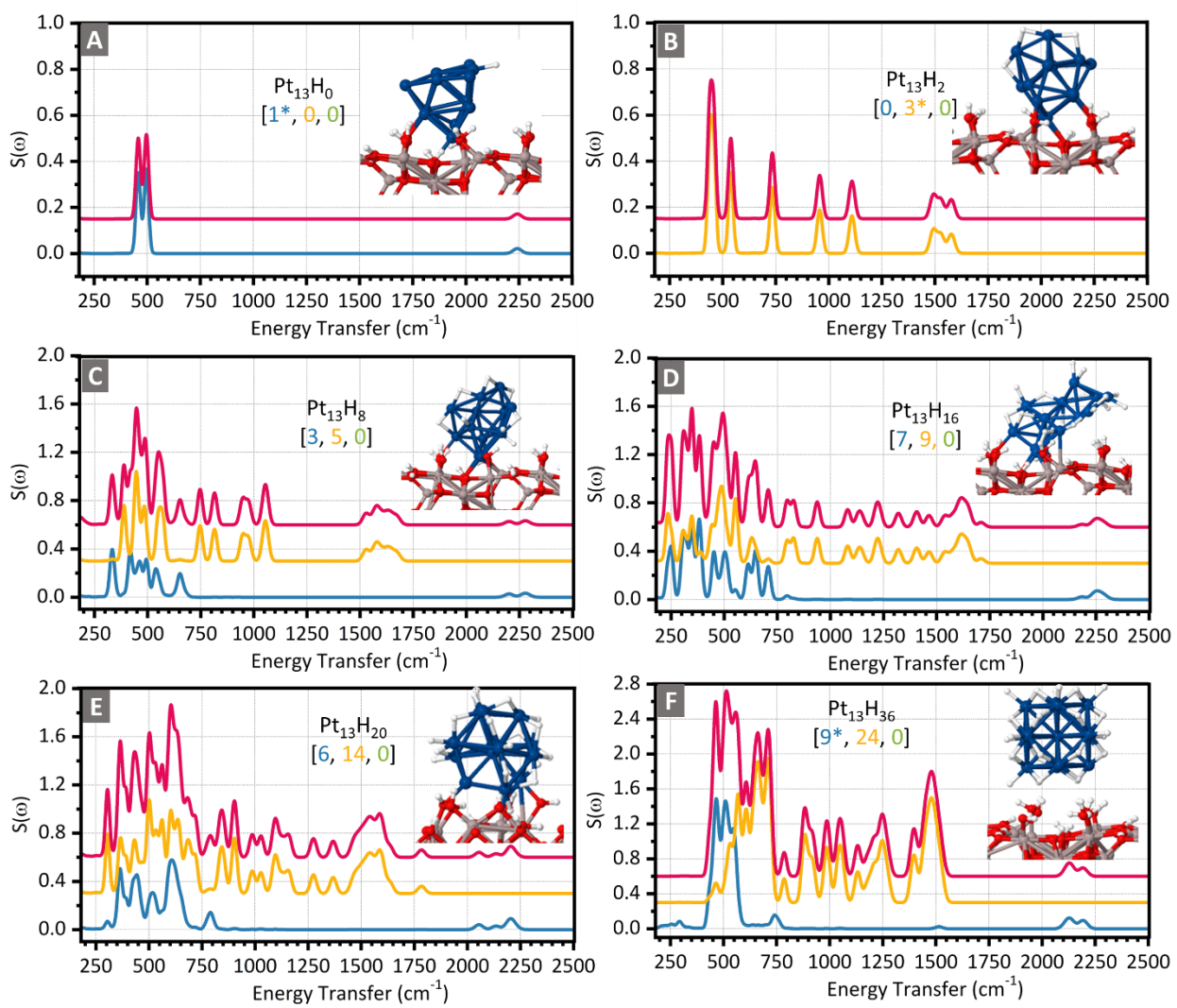

Figure S 8: simulated INS spectra of models $Pt_{13}H_0$ (A), $Pt_{13}H_2$ (B), $Pt_{13}H_8$ (C), $Pt_{13}H_{16}$ (D), $Pt_{13}H_{20}$ (E) and $Pt_{13}H_{36}$ (F) at the partially hydroxylated γ-Al_2O_3 (110) surface. The number of PtH of each type is indicated in the form [top, bridge, hollow], * indicates the occurrence of H-spillover from the support onto the nanoparticle or vice-versa.

S7: INS spectra of Pt-H species over extended Pt(100) and Pt(111) surfaces

Six different models corresponding to hydrogenated extended Pt surfaces were modelled, consisting in Pt(100) surfaces covered by bridge Pt-H species, and Pt(111) surfaces covered by top and hollow Pt-H species. For all the models, two coverages of 1 and 4 H atoms per unit cell were considered. The simulations were run with VASP[8, 9] using the PW91[10] functional and Projector Augmented Wave (PAW) pseudopotentials.[11] The surfaces were modelled as slabs containing five atomic layers, their geometries were optimised to an energy minimum (convergence threshold 0.02 eV/ Å) and their frequencies were calculated in order to simulate their INS spectra with aClimax[12] (finite differences, elongation ± 0.01 Å).

The vibrational calculations were performed at the Γ-point only. So that INS spectroscopy does not have selection rules and the vibrational modes in the whole Brillouin zone are sampled, this kind of simulation would in principle result in an only partial information. In order to retrieve the complete spectrum a whole phonon simulation on large supercell would be required, but it was deemed too computationally demanding for our means. Hence, only an explorative simulation over one 2x2 supercell of the Pt(100) surface covered by 4 bridged Pt-H per unit cell was performed, and the resulting spectrum was compared with the Γ-point one. The resulting INS spectra (Figure S 9) show some modifications in the spectral profile, with the merging of adjacent peaks into broader bands and only small shifts in the bands positions, suggesting a limited dispersion in frequency of the vibrational modes. Thus, we consider at least the signals position of the Γ-point spectra shown in Figure S 10 to be representative for the complete INS signal, allowing us to use them for a qualitative assignment.

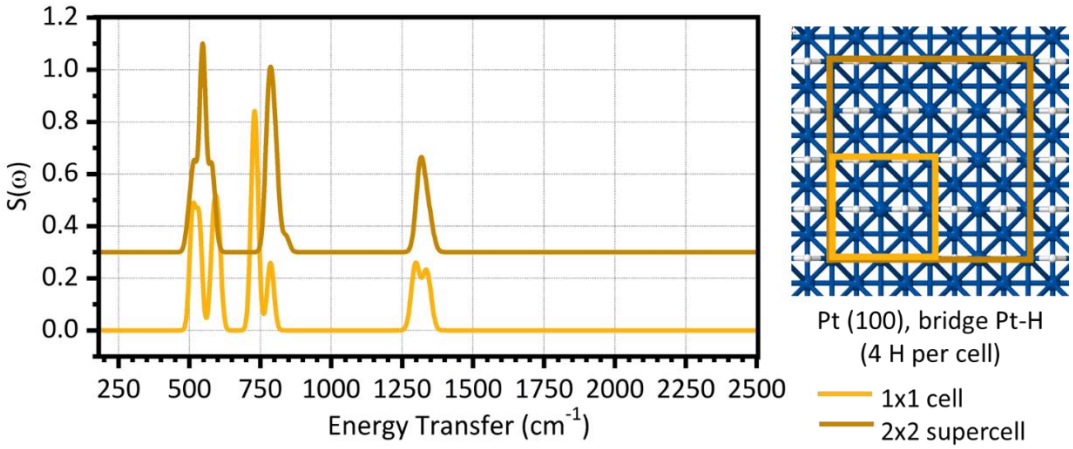

Figure S 9: comparison between the INS spectrum simulated at the Γ point and for a 2x2 supercell for the Pt(100) surface with a coverage of 4 bridge Pt-H per unit cell. The cells boundaries for the two cases are shown in the figure.

The Γ-point INS spectra simulated for the other extended Pt surfaces are shown in Figure S 10. Their spectral features can be summarised as follows:

- The simulated spectra of bridge Pt-H species at the Pt(100) surface (Figure S 10A) are characterized by few bands between 500 and 600 cm^{-1} corresponding to δ(Pt-H) modes, and by signals at about 750 and 1300 cm^{-1} attributed to ν_{as}(Pt-H) and ν_{s}(Pt-H), respectively.
- The simulated spectra of top Pt-H species at the Pt(111) surface (Figure S 10B) exhibit weak bands at about 2400 cm^{-1}, assigned to ν(Pt-H) modes, and more intense bands at energy transfer values lower than 450 cm^{-1} attributed to the δ(Pt-H) ones.

- The simulated spectra of hollow Pt-H species at the Pt(111) surface (Figure S 10C) are characterized by a series of peaks in the 850-1100 cm^{-1} range, which are attributed to their ν(Pt-H) modes.

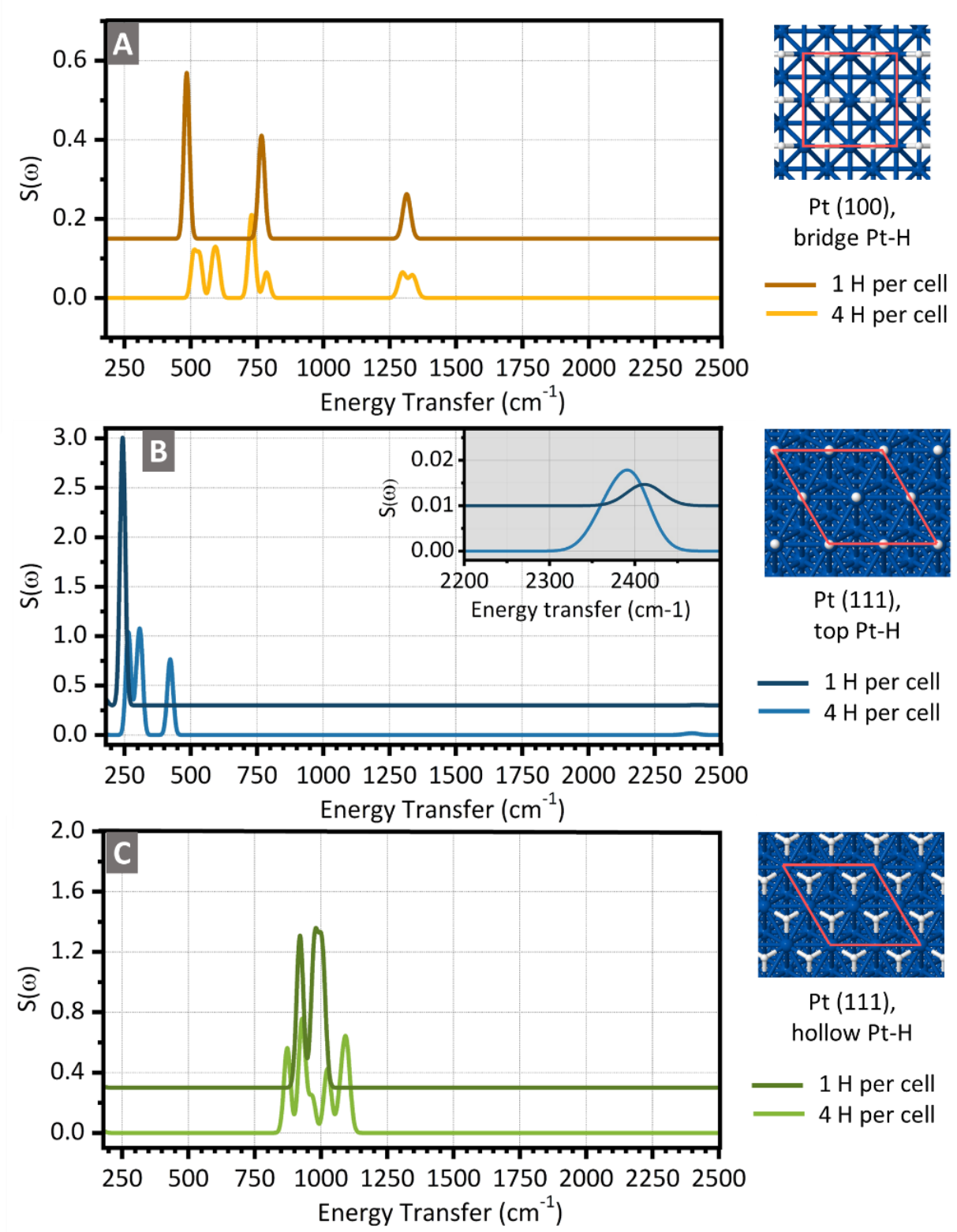

Figure S 10: simulated INS spectra for the bridge Pt-H species formed at the extended Pt(100) surface (A), the top Pt-H at the Pt(111) surface (B), and the hollow Pt-H at the Pt(111) surface (C). All the simulations are run at the Γ point only. In all the cases, H-coverages of 1 and 4 H atoms per unit cell were considered. For clarity, the surface at the highest H coverage models and the boundaries of the unit cells are shown.

S8: H-spillover in the high H-coverage experimental spectrum

We consider H-spillover to be present in our experiments when the INS band centred at about 900 cm^{-1} increases in intensity after dosing H_2 on the sample. As shown in Figure S 11, this phenomenon is not observed in the case of the experiment we performed under high H-coverage conditions (experiment (1)). Indeed, the characteristic peak for -OH groups centred at 900 cm^{-1} corresponds to a minimum in the difference spectrum which accounts for the new species formed upon interaction of the sample with H_2. We thus consider H-spillover from the Pt nanoparticles onto the support to be negligible under these experimental conditions.

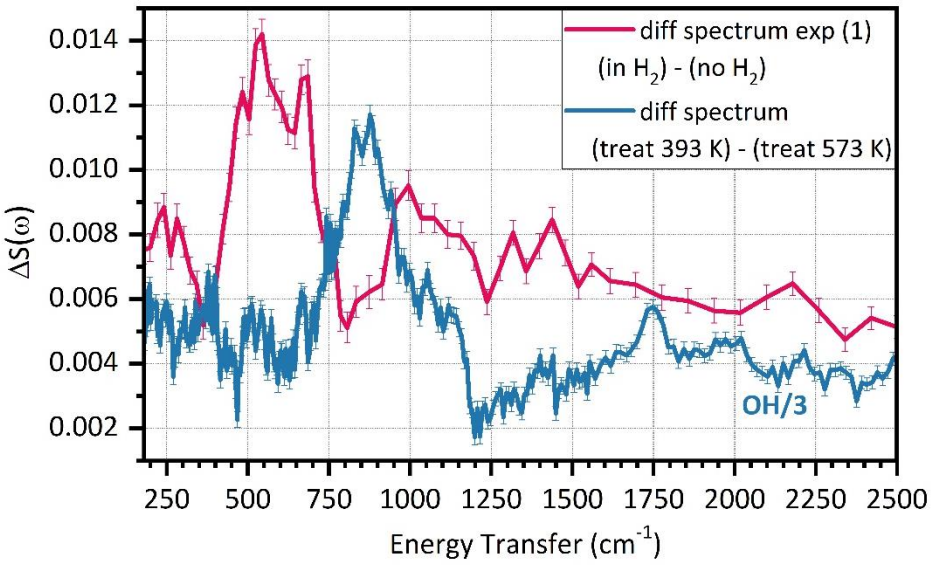

Figure S 11: Comparison between the difference INS spectrum containing the fingerprint of the H-containing species formed on the Pt/Al_2O_3 catalyst under a $P(H_2)$ = 160 mbar (red line) and the difference spectrum corresponding to the -OH species removed between the activation temperature of 393 K and 573 K.

References

1. Digne, M.; Sautet, P.; Raybaud, P.; Euzen, P.; Toulhoat, H., Hydroxyl Groups on γ-Alumina Surfaces: A DFT Study. *J. Catal.* **2002,** *211* (1), 1-5.
2. Digne, M.; Sautet, P.; Raybaud, P.; Euzen, P.; Toulhoat, H., Use of DFT to achieve a rational understanding of acid–basic properties of γ-alumina surfaces. *J. catal.* **2004,** *226* (1), 54-68.
3. Krokidis, X.; Raybaud, P.; Gobichon, A.-E.; Rebours, B.; Euzen, P.; Toulhoat, H., Theoretical Study of the Dehydration Process of Boehmite to γ-Alumina. *J. Phys. Chem. B* **2001,** *105* (22), 5121-5130.
4. Gorczyca, A.; Moizan, V.; Chizallet, C.; Proux, O.; Del Net, W.; Lahera, E.; Hazemann, J.-L.; Raybaud, P.; Joly, Y., Monitoring Morphology and Hydrogen Coverage of Nanometric Pt/γ-Al2O3 Particles by In Situ HERFD–XANES and Quantum Simulations. *Angew. Chem. Int. Ed.* **2014,** *53* (46), 12426-12429.
5. Mager-Maury, C.; Bonnard, G.; Chizallet, C.; Sautet, P.; Raybaud, P., H2-Induced Reconstruction of Supported Pt Clusters: Metal–Support Interaction versus Surface Hydride. *ChemCatChem* **2011,** *3* (1), 200-207.
6. Carosso, M.; Vottero, E.; Lazzarini, A.; Morandi, S.; Manzoli, M.; Lomachenko, K. A.; Ruiz, M. J.; Pellegrini, R.; Lamberti, C.; Piovano, A.; Groppo, E., Dynamics of Reactive Species and Reactant-Induced Reconstruction of Pt Clusters in Pt/Al2O3 Catalysts. *ACS Catal* **2019,** *9* (8), 7124-7136.
7. Scott, A. P.; Radom, L., Harmonic Vibrational Frequencies: An Evaluation of Hartree−Fock, Møller−Plesset, Quadratic Configuration Interaction, Density Functional Theory, and Semiempirical Scale Factors. *J. Phys. Chem.* **1996,** *100* (41), 16502-16513.
8. Kresse, G.; Hafner, J., Ab initio molecular-dynamics simulation of the liquid-metal--amorphous-semiconductor transition in germanium. *Phys. Rev. B* **1994,** *49* (20), 14251-14269.
9. Kresse, G.; Furthmüller, J., Efficient iterative schemes for ab initio total-energy calculations using a plane-wave basis set. *Phys. Rev. B* **1996,** *54* (16), 11169-11186.
10. Perdew, J. P.; Burke, K.; Ernzerhof, M., Generalized Gradient Approximation Made Simple. *Phys. Rev. Lett.* **1996,** *77* (18), 3865-3868.
11. Kresse, G.; Joubert, D., From ultrasoft pseudopotentials to the projector augmented-wave method. *Phys. Rev. B* **1999,** *59* (3), 1758-1775.
12. Ramirez-Cuesta, A. J., aCLIMAX 4.0.1, The new version of the software for analyzing and interpreting INS spectra. *Comput. Phys. Commun.* **2004,** *157* (3), 226-238.